Science of the Total Environment 755 (2021) 142487

Contents lists available at ScienceDirect

Science of the Total Environment

journal homepage: www.elsevier.com/locate/scitotenv

Elucidating controls on cyanobacteria bloom timing and intensity via Bayesian mechanistic modeling

Dario Del Giudice [a,*], Shiqi Fang [a], Donald Scavia [b], Timothy W. Davis [c], Mary Anne Evans [d], Daniel R. Obenour [a,e]

[a] Department of Civil, Construction & Environmental Engineering, NC State University, Raleigh, NC 27695, USA
[b] School for Environment and Sustainability, University of Michigan, Ann Arbor, MI 48104, USA
[c] Department of Biological Sciences, Bowling Green State University, Bowling Green, OH 43403, USA
[d] U.S. Geological Survey, Great Lakes Science Center, Ann Arbor, MI 48105, USA
[e] Center for Geospatial Analytics, NC State University, Raleigh, NC 27695, USA

HIGHLIGHTS

- We develop a Bayesian biophysical model to understand harmful algal bloom dynamics.
- With a high-resolution dataset, we find bloom onset occurs after a month of $T > 20$ °C.
- Model comparisons indicate reduced grazing is the primary driver of bloom accrual.
- 2 °C warming may lead blooms to start about 10 days earlier and be 23% more intense.

GRAPHICAL ABSTRACT

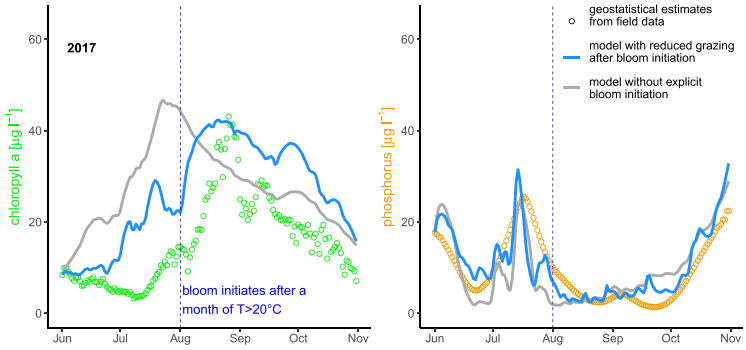

ARTICLE INFO

Article history:
Received 30 March 2020
Received in revised form 17 September 2020
Accepted 17 September 2020
Available online 24 September 2020

Editor: Ouyang Wei

Keywords:
Eutrophication
Harmful algal blooms
Bayesian inference
Process-based modeling
Great Lakes
Hindcasts and projections

ABSTRACT

The adverse impacts of harmful algal blooms (HABs) are increasing worldwide. Lake Erie is a North American Great Lake highly affected by cultural eutrophication and summer cyanobacterial HABs. While phosphorus loading is a known driver of bloom size, more nuanced yet crucial questions remain. For example, it is unclear what mechanisms are primarily responsible for initiating cyanobacterial dominance and subsequent biomass accumulation. To address these questions, we develop a mechanistic model describing June–October dynamics of chlorophyll *a*, nitrogen, and phosphorus near the Maumee River outlet, where blooms typically initiate and are most severe. We calibrate the model to a new, geostatistically-derived dataset of daily water quality spanning 2008–2017. A Bayesian framework enables us to embed prior knowledge on system characteristics and test alternative model formulations. Overall, the best model formulation explains 42% of the variability in chlorophyll *a* and 83% of nitrogen, and better captures bloom timing than previous models. Our results, supported by cross validation, show that onset of the major midsummer bloom is associated with about a month of water temperatures above 20 °C (occurring 19 July to 6 August), consistent with when cyanobacteria dominance is usually reported. Decreased phytoplankton loss rate is the main factor enabling biomass accumulation, consistent with reduced zooplankton grazing on cyanobacteria. The model also shows that phosphorus limitation is most severe in August, and nitrogen limitation tends to occur in early autumn. Our results highlight the role of temperature in regulating bloom initiation and subsequent loss rates, and suggest that a 2 °C increase could lead to blooms that start about 10 days earlier and grow 23% more intense.

* Corresponding author.
E-mail address: ddelgiu@ncsu.edu (D. Del Giudice).

https://doi.org/10.1016/j.scitotenv.2020.142487
0048-9697/

1. Introduction

Harmful algal blooms (HABs) refer to the rapid proliferation and accumulation of toxic or otherwise noxious algae (Anderson et al., 2012). Cyanobacteria, also known as cyanophyta or blue-green algae, cause some of the most common and severe freshwater impairments. In particular, toxin-forming cyanobacteria genera can lead to poisoning of fishes, livestock, and humans (Carmichael and Boyer, 2016), affecting the liver, kidney, and the central nervous system (Carmichael, 2001; Milutinović et al., 2003). In addition to these health consequences, HABs can also have adverse economic impacts (Hoagland et al., 2002; Steffensen, 2008). The global increase in HABs has been reported since at least the 1980s (Anderson et al., 2012), and the trend is likely to persist in the next decades (Huisman et al., 2018).

Eutrophication and climate warming appear to be two broad causes of increasing blooms in aquatic ecosystems (O'Neil et al., 2012). The former refers to the increase in anthropogenic nutrient inputs that tend to stimulate growth of algae. While phosphorus (P) appears to be the key nutrient driver in many freshwater systems (Carpenter, 2008; Schindler et al., 2016), nitrogen (N) also plays a role (Gobler et al., 2016; Newell et al., 2019). Climate warming also favors HAB development (Carey et al., 2012; Chapra et al., 2017; Kosten et al., 2012) through a variety of potential mechanisms related to bloom initiation and accumulation, including higher cyanobacteria growth rates (Paerl and Otten, 2013) and reduced grazing pressure associated with a decrease in zooplankton body size (Lürling et al., 2013; Moore and Folt, 1993).

The Laurentian Great Lakes are the largest freshwater system in the world by surface area and toxic blooms occur regularly in different parts of the system, including portions of lakes Michigan, Huron, Ontario, and Erie (Carmichael and Boyer, 2016). Lake Erie (LE), the warmest and most eutrophic Great Lake, has been particularly affected by HABs, especially in its western basin (Bullerjahn et al., 2016; Michalak et al., 2013; Jankowiak et al., 2019; Watson et al., 2016) near the Maumee River outlet (Fig. 1) (Bridgeman et al., 2013). It is generally there that blooms originate (Bridgeman et al., 2012) and are most intense (Jankowiak et al., 2019). Nutrient loading from the Maumee River is widely considered to be the main driver of LE HABs (Chaffin et al., 2014; Obenour et al., 2014; Stumpf et al., 2012). This area of the lake also has the highest observed cyanobacteria growth rates (Chaffin et al., 2011) and blooms there led to a "do not drink" advisory for the Toledo water supply in 2014 (Steffen et al., 2017). Thus, understanding algal dynamics in this region is essential to water resources management.

Models of different complexity and resolution have been developed to understand and predict algal blooms in LE (Arhonditsis et al., 2019). Simple empirical models have generally focused on interannual variability of maximum HAB size (e.g., biomass). Models of this type helped determine the importance of springtime P loads from the Maumee River in driving summertime bloom magnitude (Bertani et al., 2017; Obenour et al., 2014; Stumpf et al., 2012), and inform governments on appropriate nutrient reduction targets (Scavia et al., 2016) as well as impairment designations (Davis et al., 2019). At the other end of the modeling spectrum, complex mechanistic models (typically with hundreds of nodes and dozens of parameters) have been used to study LE phytoplankton dynamics in greater detail (Jiang et al., 2015; Leon et al., 2011; Verhamme et al., 2016; Zhang et al., 2008).

The mechanistic model of Verhamme et al. (2016) has been compared against the longest monitoring period (five years of data) and has also been used to evaluate nutrient loading targets for western LE (Scavia et al., 2016). However, this state-of-the-art model tends to initiate the midsummer bloom four weeks too early (Verhamme et al., 2016). This deficiency is linked to a puzzling lag between high late-spring P concentrations (~early June) and midsummer bloom initiation (~late July) (Conroy et al., 2014; Newell et al., 2019; Stumpf et al., 2012). Some field (De Stasio et al., 2018; Twiss et al., 2014) and modeling studies (e.g., Jiang et al., 2015) suggest that reduced algal grazing may explain the blooms, yet other studies point to higher algal growth rates (Davis et al., 2012; Gobler et al., 2008; Verhamme et al., 2016). Additional potential mechanisms include water column stratification and algal buoyancy, which allow cyanobacteria to outcompete other algal taxa for light (Paerl and Otten, 2013) although the shallow regions of western LE are not consistently stratified in summer (Bosse et al., 2019).

Overall, critical questions remain: i) what environmental conditions drive cyanobacteria dominance and bloom initiation in midsummer? ii) what mechanisms explain both low chlorophyll in early summer and rapid algal accumulation following bloom initiation? and iii) how strongly will algal bloom timing and severity respond to climate warming? In this study, bloom initiation is defined as the onset of the main (i.e., largest) midsummer bloom, and as discussed by Anderson et al. (2012), is associated with a rapid accumulation of algal biomass (Section 2.3). The goals of this study are to probabilistically test hypotheses about mechanisms of bloom biomass accumulation, and to predict the timing of bloom initiation based on environmental drivers. We use a unique set of tools to address these objectives: a new parsimonious yet process-based model for simulating nutrient and chlorophyll dynamics, a recently-developed high-resolution (daily) geostatistical calibration dataset (2008–2017) (Fang et al., 2019), and a rigorous Bayesian inference framework for parameter (e.g., rate) estimation.

2. Materials and methods

2.1. Study area and data

We focus on the area within 20 km of the Maumee River outlet, which generally suffers the most severe blooms and has been heavily monitored (Bosse et al., 2019; Chaffin et al., 2014). We refer to this area (Fig. 1), which has a surface area $A = 271$ km^2 and average depth $h = 2.96$ m, as the Maumee Proximal Area (MPA), to distinguish it from the smaller Maumee Bay and the larger western basin of LE. MPA is an ideal area to focus on the influence of the Maumee River because it corresponds approximately to the largest area with limited influence from the Detroit and Raisin River discharges (Bridgeman et al., 2013; Chaffin et al., 2011).

Lake concentration data for model calibration include chlorophyll *a* (chl), dissolved reactive P (DRP), and dissolved inorganic N (DIN) that includes nitrate plus nitrite (NO_x) and ammonia (NH_3). Secchi depth was used to estimate light attenuation as a function of chl (Section S1). The data have been synthesized from multiple institutions including University of Toledo, The Ohio State University, Environment and Climate Change Canada, US Geological Survey (USGS), and the National Oceanic and Atmospheric Administration (NOAA) through a geostatistical method that generates daily time series of average water column concentrations for the study domain (Fang et al., 2019). Fang et al. (2019) found that, despite differences among the sampling programs, they could be reasonably combined using statistical adjustments. The comparability of water quality data across programs is also supported by side-by-side methods tests (Golnick et al., 2016). More information on these data is provided in the Section S2 and the actual estimates are displayed in the Results (Section 3.1).

River inputs include observed discharge (Q), and concentrations of DRP, NO_x, NH_3, and Total Kjeldahl N (TKN) obtained from Heidelberg University's National Center for Water Quality Research (NCWQR, https://ncwqr.org/monitoring/data/), aggregated to daily values. Gaps in Heidelberg Q data are filled using a regression based on USGS Q data (USGS, https://waterdata.usgs.gov/usa/nwis/uv?site_no=04193500). Gaps in DRP and NO_x data were filled using linear interpolation. For DRP, only 5.8% of days were missing between 2008 and 2017, with the length of each missing period being about 3 days. River chl data were collected by USGS during 2016–2017 and NH_3 data were collected on a weekly basis by NCWQR. Both NH_3 and chl were imputed across all days based on regressions with other river concentration data from NCWQR (Section S3). As model sensitivity to riverine chl and NH_3 is low (see Section 3.5), imputation uncertainty is expected

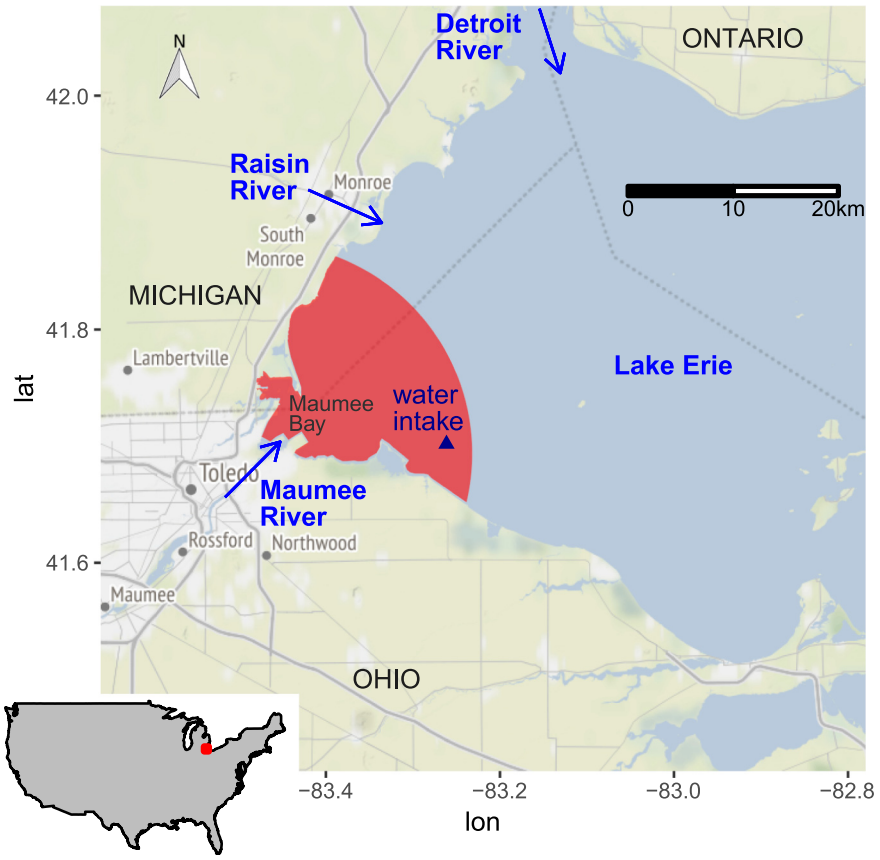

Fig. 1. Maumee Proximal Area (red) in western Lake Erie, showing river outlets and Toledo drinking water intake. (For interpretation of the references to colour in this figure legend, the reader is referred to the web version of this article.)

to have a negligible impact. Note that this is the first modeling study of Lake Erie to directly use NH_3 data (which averages about 4% of riverine TKN) as a component of the dissolved inorganic N load, thus taking into explicit account an important source of highly bioavailable N (Newell et al., 2019).

Other environmental data include daily water temperature (T [°C]) from NOAA (CoastWatch, https://coastwatch.glerl.noaa.gov/statistic/statistic.html), solar insolation on a horizontal surface (I [MJ m^{-2} d^{-1}]) from NASA (POWER, https://power.larc.nasa.gov/), solar elevation above the horizon β [rad] and photoperiod f (fraction of day from sunrise to sunset) from the suncalc package (Thieurmel and Elmarhraoui, 2019), lake water level from NOAA (https://tidesandcurrents.noaa.gov/stationhome.html?id=9063085), and wind speed from NOAA (NDBC, https://www.ndbc.noaa.gov) processed as in Fang et al. (2019).

2.2. Baseline mechanistic model (M_0)

The data described above were used to update (i.e., calibrate) mechanistic model parameters through Bayesian inference (e.g., Sikorska et al., 2015; Villez et al., 2020). The model was developed in stages, consistent with previous eutrophication studies testing mechanisms potentially relevant to improving system representation (Katin et al., 2019; Sadeghian et al., 2018) and with the concept of "gradual incorporation of complexity" recommended by Shimoda and Arhonditsis (2016). This section describes the baseline mechanistic model (M_0) while Section 2.3 describes candidate model enhancements.

Model M_0 represents daily dynamics of chl, DRP, DIN, and nonalgal biomass (Z). DIN was included because there is evidence of N limitation in the MPA at the end of summer in some years (Chaffin et al., 2014, 2013, 2011), indicating it plays a relevant role in LE phytoplankton dynamics (Newell et al., 2019; Salk et al., 2018). The model represents the MPA as a continuously stirred tank reactor with flow regulated by the Maumee River discharge. Nutrient loads from the river mix into the lake and are incorporated into chl, a common surrogate for algal biomass (Chapra, 2008; Arhonditsis et al., 2019; Fang et al., 2019). Algae die because of grazing and other causes and their biomass gets incorporated into suspended zooplankton and organic detritus (Z). Finally, Z (represented in units of N equivalents) decomposes and releases the nutrients stoichiometrically back into the water. In the baseline model version (M_0), differential equations for chl (a), DRP (p), DIN (n) and Z (z) are:

$$\frac{da}{dt} = (a_{riv} - a)\frac{Q_{riv}}{V} + \phi_L \phi_N 1.066^{T-20} k_g a - k_l a \quad (1)$$

$$\frac{dp}{dt} = (p_{riv} - p)\frac{Q_{riv}}{V} - r_{pa}\phi_L \phi_N 1.066^{T-20} k_g a + k_m 1.08^{T-20} z \frac{a_{pa}}{a_{na}} + B 1.08^{T-\bar{T}} \quad (2)$$

$$\frac{dn}{dt} = (n_{riv} - n)\frac{Q_{riv}}{V} - r_{na}\phi_L \phi_N 1.066^{T-20} k_g a + k_m 1.08^{T-20} z - k_d n \quad (3)$$

$$\frac{dz}{dt} = (z_{riv} - z)\frac{Q_{riv}}{V} + r_{na} k_l a - \frac{\nu_s}{h} z - k_m z 1.08^{T-20} \quad (4)$$

where k_l [d^{-1}] is the loss rate of phytoplankton representing grazing and other causes of mortality such as viral lysis, k_g [d^{-1}] is the maximum algal growth rate, ϕ_L is light limitation, ϕ_N is nutrient limitation, ν_s [m d^{-1}] is the settling velocity of Z, B [μg l^{-1} d^{-1}] represents the internal DRP load from the bottom sediments, r_{pa} [μg μg^{-1}] is the algal phosphorus-to-chlorophyll ratio, r_{na} [μg μg^{-1}] is the algal nitrogen-to-

chlorophyll ratio, k_m [d^{-1}] is the rate of mineralization of Z, and k_d [d^{-1}] is the rate of denitrification and related N dissimilatory processes (Salk et al., 2018). In Eq. (4), z_{riv} is the portion of TKN which is not NH_3 nor algal biomass ($a_{riv}\, r_{na}$). Temperature adjustments for growth, mineralization, and sediment loading are based on typical Arrhenius formulations (Chapra, 2008). V represents the domain volume which is calculated as $V = Ah$, taking into account fluctuations in lake depth (h). Nutrient limitation, ϕ_N, is represented using a Monod formulation and Liebig's Law of the Minimum (Sadeghian et al., 2018):

$$\phi_N = min\left(\frac{p}{S_p + p}, \frac{n}{S_n + n}\right) \tag{5}$$

where S_p and S_n are the half-saturation concentrations [μg l^{-1}] for DRP and DIN, respectively.

Light limitation, ϕ_L, is estimated based on the formulation proposed by Steele (1965) integrated over the water column using the Beer-Lambert Law for light attenuation (Chapra, 2008):

$$\phi_L = \frac{2.7f}{k_e h_a}\left(exp\left(-\frac{I_a}{I_s}\, exp(-k_e h_a)\right) - exp\left(-\frac{I_a}{I_s}\right)\right) \tag{6}$$

where I_a is the daily average photosynthetically available light, about 45% of the incoming radiation (Britton and Dodd, 1976; Chapra, 2008), and I_s is the optimal photosynthetically available light intensity set to 7.2 [MJ m^{-2} d^{-1}] based on preliminary analysis of chl versus I and consistent with typical values (Chapra, 2008). Finally, k_e [m^{-1}] is the light attenuation coefficient, which is a function of chl (Section S1).

2.3. Enhancing the model to explicitly consider blooms

We test multiple model enhancements designed to improve the representation of water quality dynamics relative to the baseline model M_0 (Fig. 2). Specifically, we test three models that allow parameters to vary before and after bloom initiation: M_l allows for a variable loss rate (k_l), M_g allows for a variable maximum growth rate (k_g), and $M_{l,g}$ allows for both the growth and loss rates to vary. These rate parameters are estimated both before (k_g, k_l) and after ($k_{g,b}$, $k_{l,b}$) bloom initiation using data-driven Bayesian inference (Section 2.4). By comparing which model enhancements lead to greater fidelity between observed and predicted water quality conditions, we are able to assess which processes are most critical to bloom initiation and accumulation.

Here, bloom initiation is defined as the beginning of rapid biomass accumulation associated with the main (i.e., largest) midsummer MPA bloom event for each year. Due to the noisiness of phytoplankton data, exact bloom initiation dates are difficult to define, and we thus initially employ a nominal initiation date of 24 July, consistent with large-scale studies showing bloom formation typically begins in late July (Fang et al., 2019; Stumpf et al., 2012, 2016). Importantly, late July is also the period during which cyanobacteria typically become dominant based on *in situ* measurements (Bosse et al., 2019; Bridgeman et al., 2012) and remote sensing (Stumpf et al., 2012, 2016). Note that there is a strong correlation between geostatistical (chl-based) estimates and remote sensing estimates of maximum cyanobacterial bloom size (Fang et al., 2019). For these reasons, bloom initiation is approximately synonymous with a shift to cyanobacteria dominance.

After determining which model (M_l, M_g, or $M_{l,g}$) best explains the variability in the observations assuming a fixed bloom initiation date, we explore the potential to further improve model performance by allowing the initiation date to vary based on an environmental trigger. To assess potential environmental triggers, we compare June–October distributions of factors thought to influence cyanobacteria dominance (Bertani et al., 2017; Paerl and Otten, 2013) with their distribution during the second half of July (i.e., the period around 24 July). We screen daily water temperature, discharge, wind speed, and irradiance using both visual inspection and Kolmogorov–Smirnov tests to assess how the two distributions are different. The variable with the strongest difference is identified as the trigger variable, and we use a trigger threshold value that corresponds to the late-July distribution and literature (Section 3.3). In addition, a timing parameter, τ, is included to assess the number of consecutive days the threshold must be exceeded before bloom initiation occurs.

2.4. Bayesian model calibration

Each model was calibrated through Bayesian inference, which combines prior knowledge on model parameters (as probability distributions, $f(\boldsymbol{\theta})$) and information from observations (in this case, the geostatistically-derived water quality conditions for the MPA), as described by the likelihood function, $L = f(\mathbf{y_o}|\boldsymbol{\theta})$. The result is the updated posterior distribution of calibrated parameters, $f(\boldsymbol{\theta}|\mathbf{y_o})$. Bayesian inference is numerically implemented using adaptive Metropolis sampling

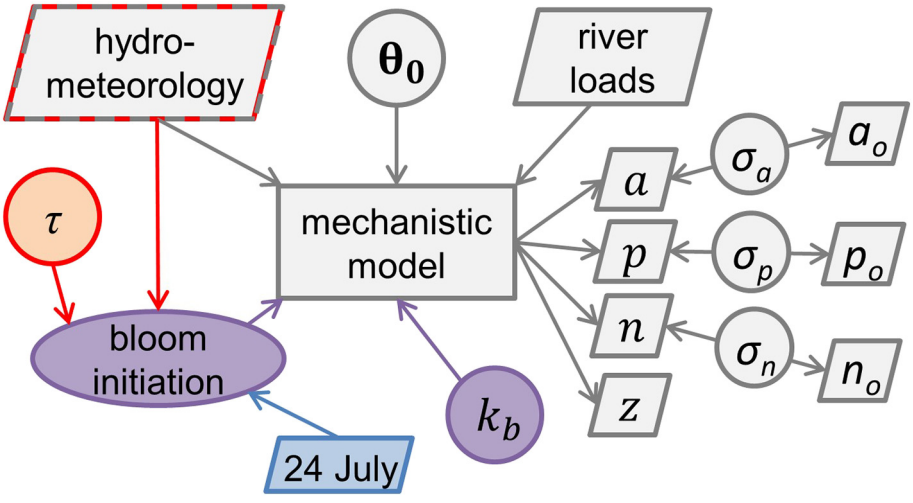

Fig. 2. Model schematic where inputs/outputs are shown as parallelograms and estimated parameters are shown as circles. Core components of the baseline model (M_0) are shown in gray, including baseline mechanistic rate parameters ($\boldsymbol{\theta_0}$). Calibration data are distinguished from predictions with subscript 'o' (for observation). Enhancements associated with variable-rate models (M_l, M_g, or $M_{l,g}$) are shown in purple, where k_b represents the varied rate ($k_{l,b}$, $k_{g,b}$, or both). Blue components are associated with a fixed (i.e., nominal) bloom initiation date, whereas red components allow for a model-determined initiation date based on a hydro-meteorological variable and timing parameter τ. (For interpretation of the references to colour in this figure legend, the reader is referred to the web version of this article.)

Table 1
Prior information on parameters calibrated through Bayesian inference. All parameters have a lower bound of 0, as negative values are physically implausible. Prior distributions are characterized by mean (μ) and standard deviation (σ), both referring to the normal distribution, N(μ,σ) before truncation.

Parameter	Prior distribution	Source
Max. growth rate, k_g [d^{-1}]	N(1.5,0.5)	(Dietzel and Reichert, 2014; Leon et al., 2011; Zhang et al., 2008)
Loss rate, k_l [d^{-1}]	N(0.25,0.125)	(Chapra, 2008)
P-to-chl ratio, r_{pa} [μg μg^{-1}]	N(1.5,0.15)	(Chapra, 2008)
N-to-chl ratio, r_{na} [μg μg^{-1}]	N(7.2,0.72)	(Chapra, 2008)
Denitrification rate, k_d [d^{-1}]	N(0.05,0.025)	(Zhang et al., 2008)
Mineralization rate, k_m [d^{-1}]	N(0.11,0.11)	(Dietzel and Reichert, 2014; Zhang et al., 2008; Sadeghian et al., 2018)
Effective settling velocity, v_s [m d^{-1}]	N(0.11,0.13)	(Chapra et al., 2017; Leon et al., 2011)
Half-saturation conc. for DRP, S_p [μg l^{-1}]	N(3.0,1.0)	(Chapra, 2008; Zhang et al., 2008)
Half-saturation conc. for DIN, S_n [μg l^{-1}]	N(15,2.5)	(Chapra, 2008; Verhamme et al., 2016)
Diffusive DRP flux, B [μg l^{-1} d^{-1}]	N(0.46,0.07)	(Matisoff et al., 2016)
Timing parameter, τ [d]	N(30,15)	(Bertani et al., 2017)

(Del Giudice et al., 2013; Haario et al., 2001). Analyses are performed in R (www.R-project.org/) and the model differential equations are integrated using the package odin (FitzJohn, 2019).

Prior information on mechanistic parameters is represented by normal distributions (Table 1). In addition, these distributions are truncated at zero to avoid unrealistic, negative rates. Error parameters (σ_a, σ_n, σ_p) are in the same units as the transformed output and are assigned a uniform probability distribution over positive real numbers.

The likelihood function is used to learn from the observations and to evaluate the match between model and observations for a given parameter set (Section S4). The likelihood is defined in a transformed space to address heteroscedasticity (i.e., the tendency for uncertainties to be higher when concentrations are higher). Here, we use a square-root transformation (Section S5) similar to previous water quality studies involving Bayesian inference (Del Giudice et al., 2018a, 2018b; Sikorska et al., 2015). Additionally, the likelihood function, model output, and data were compared as 10-day averages determined at 10-day intervals (reducing the number of observations by a factor of 10) to help account for the reduced information content of autocorrelated data (Westra et al., 2014). Consistent with this approach, the R^2 (i.e., coefficient of determination based on the ratio of residual square error to total square error around the mean, Faraway, 2015) values discussed hereafter also refer to averaged data at 10-day intervals.

3. Results and discussion

3.1. Lake Erie observations

Average MPA concentrations obtained through geostatistical analysis of *in situ* data show recurring summertime patterns (Fig. 3). Both river and lake DRP concentrations are high and chl concentrations are low in early summer. P concentrations appear particularly high in 2015, which had the largest observed June discharge and DRP loads in the studied decade. The average date of bloom initiation and cyanobacterial dominance suggested by the literature (24 July, Section 2.3) approximately corresponds to the observed beginning of the main midsummer bloom. At that time, nutrient concentrations are low and DRP reaches its minimum shortly thereafter (on average, on 12 August). Early-summer DRP peaks precede chl peaks by approximately two months (on average, 68 d) and bloom initiation by about 40 d. Thus, this study quantifies ecological lags that have been discussed qualitatively in previous literature (Conroy et al., 2014; Newell et al., 2019).

3.2. Simulations with baseline and enhanced bloom models

The different mechanistic models simulate observed algal and nutrient patterns with varying degrees of success (Table 2). The baseline

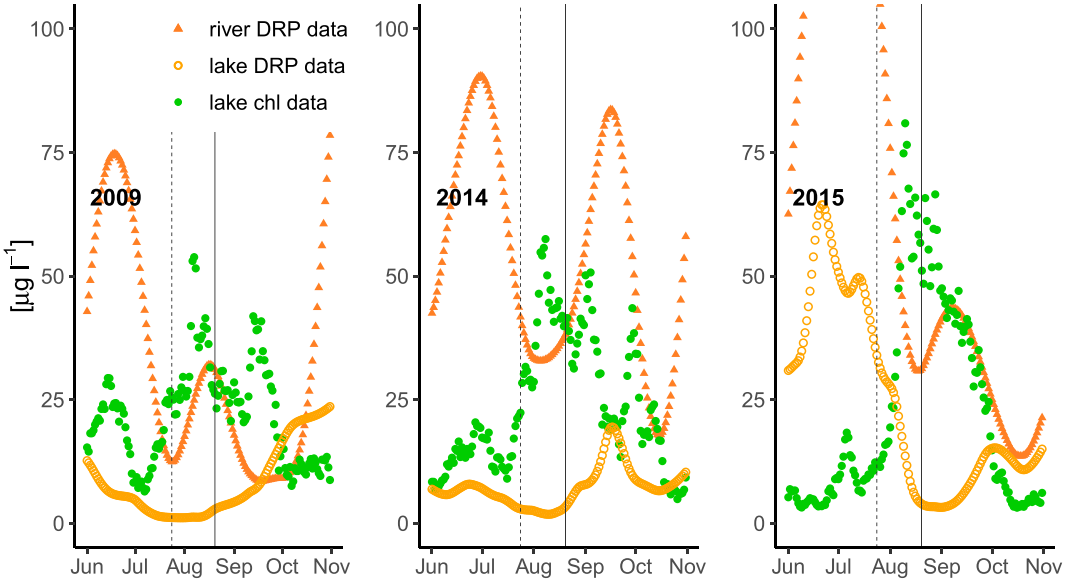

Fig. 3. Time series of chl and main limiting nutrient (DRP) concentrations for years with low (2009), average (2014), and severe (2015) blooms. Lacustrine observations are estimated from sampling data using the method of Fang et al. (2019). Riverine DRP observations are smoothed for better visualization using a Gaussian function with window = 50 d. Note that some 2015 DRP values exceed the upper limit of the y-axis. The vertical lines indicate 24 July and 20 August, which are the nominal bloom initiation date from the literature (dashed) and the average peak bloom date based on our data (solid) across all years (see Fig. S1 for all years).

Table 2
Results of the modeling experiments in terms of coefficient of determination (R^2) for chlorophyll, DRP, and DIN; overall log-likelihood; and parameter estimates for algal growth (k_g) and loss (k_l) rates. Parameters with '*b*' subscript indicate the shifted rate, following cyanobacteria bloom initiation. For each parameter, the mode and standard deviation (in parentheses) of the marginal posterior distribution is provided. Note that the last row is for a model with a temperature-mediated bloom initiation date (Section 3.3).

Model	R^2_{chl}	R^2_p	R^2_n	log-L	k_l [d^{-1}]	$k_{l,b}$ [d^{-1}]	k_g [d^{-1}]	$k_{g,b}$ [d^{-1}]
M_0	0.04	0.27	0.83	−2133	0.05 (0.01)	NA	0.70 (0.07)	NA
M_g	0.15	0.28	0.83	−2125	0.12 (0.02)	NA	1.03 (0.13)	2.09 (0.37)
M_l	0.37	0.38	0.82	−2100	0.30 (0.04)	0.11 (0.01)	1.81 (0.21)	NA
$M_{l,g}$	0.37	0.40	0.82	−2098	0.26 (0.05)	0.10 (0.02)	1.68 (0.22)	1.80 (0.35)
$M_{l,T}$	0.42	0.39	0.83	−2090	0.32 (0.05)	0.11 (0.01)	1.94 (0.23)	NA

model (M_0) with constant parameters has negligible explanatory power for chl relative to the mean (i.e., $R^2 = 0.04$), yet it explains 27% of DRP variability and 83% of DIN variability. Simulated blooms start in early June when nutrients are high, rather than in late July, and blooms peak on average on 25 July, as opposed to the observed average peak date of 20 August. The enhanced model (M_g) that allows the phytoplankton growth rate, k_g, to change after the nominal bloom initiation date explains 15% of chl variability and 28% of DRP variability, while providing similar predictive skill for DIN (relative to M_0). Alternatively, allowing for a modified loss rate, k_l, following bloom initiation (M_l) results in even better predictive performance (explaining 37% and 38% of chl and DRP variability, respectively). Furthermore, model M_l accurately reproduces the nutrient-chl lag, while M_g simulates chl maxima about 16 days too early.

Finally, the model that includes both variable growth and loss rates ($M_{l,g}$) has approximately the same skill (R^2) and overall likelihood (log-L, representing model skill across all three calibration variables: chl, DRP, and DIN) as M_l despite the additional parameter. The posterior parameter distribution for $M_{l,g}$ shows a non-significant increase in $k_{g,b}$ compared to k_g (probability of overlap, $p = 0.5$). At the same time, $M_{l,g}$ shows a significant 65% decrease in phytoplankton loss rate once blooms initiate ($p < 0.001$), similar to M_l. Consequently, model M_l is found to be preferable to M_g and $M_{l,g}$. In general, the results show that a model with lower late-summer algal mortality, consistent with observed shifts in phytoplankton community composition to cyanobacteria, successfully captures the temporal lag between nutrient inputs and the late-summer bloom.

3.3. Predicting bloom initiation date

The analyses in the previous section were based on a nominal bloom initiation date of 24 July (Fig. 2, blue). Here, we explore the predictability of bloom initiation based on an environmental driver (Fig. 2, red), which allows for the initiation date to vary across years and potentially better captures the timing of the rapid increase in biomass associated with the mid-summer bloom. Both visual inspection and test results, comparing summer-wide vs. late-July distributions of potentially relevant environmental variables, show that temperature, *T*, has the most distinctive late-July distribution (Fig. 4). Also, we note that late-July *T* is continuously above 20 °C, consistent with LE studies showing that blooms tend to be associated with temperatures exceeding approximately 20 °C (Bertani et al., 2017; Stumpf et al., 2012, 2016).

Selecting temperature as a trigger of bloom initiation, associated with a transition to cyanobacteria dominance, we develop the final model ($M_{l,T}$). Model calibration (Fig. S2, parameter τ) indicates that about 32 consecutive days of water temperatures above 20 °C is required to trigger a change in loss rate (k_l). Based on this formulation, predicted bloom initiation dates range from 19 July (in 2012, a year with a warm summer) to 6 August (in 2015). This final model variant explains 42% of chl variability (Fig. 5), compared to 37% using the nominal initiation date of 24 July (M_l, Table 2). Moreover, compared to the original model with constant rate parameters (M_0), absolute improvements in variance explained are 12% for DRP and 38% for chl.

Overall, this temperature-based formulation addresses a gap in previous HAB modeling research regarding bloom initiation (Stumpf

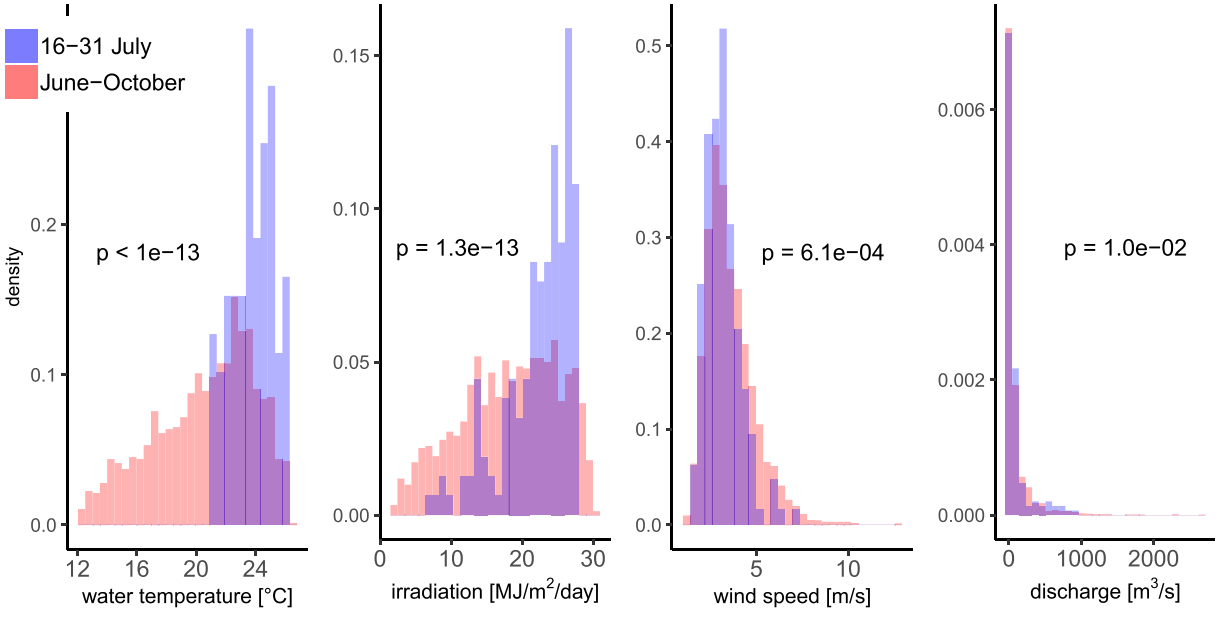

Fig. 4. Observed probability distributions of candidate predictors of bloom initiation date ordered based on the degree to which late-July distributions deviate from June–October distributions. Deviations are assessed based on visual inspection and the Kolmogorov–Smirnov test, where lower *p*-values indicate a higher confidence in the distributions being significantly different.

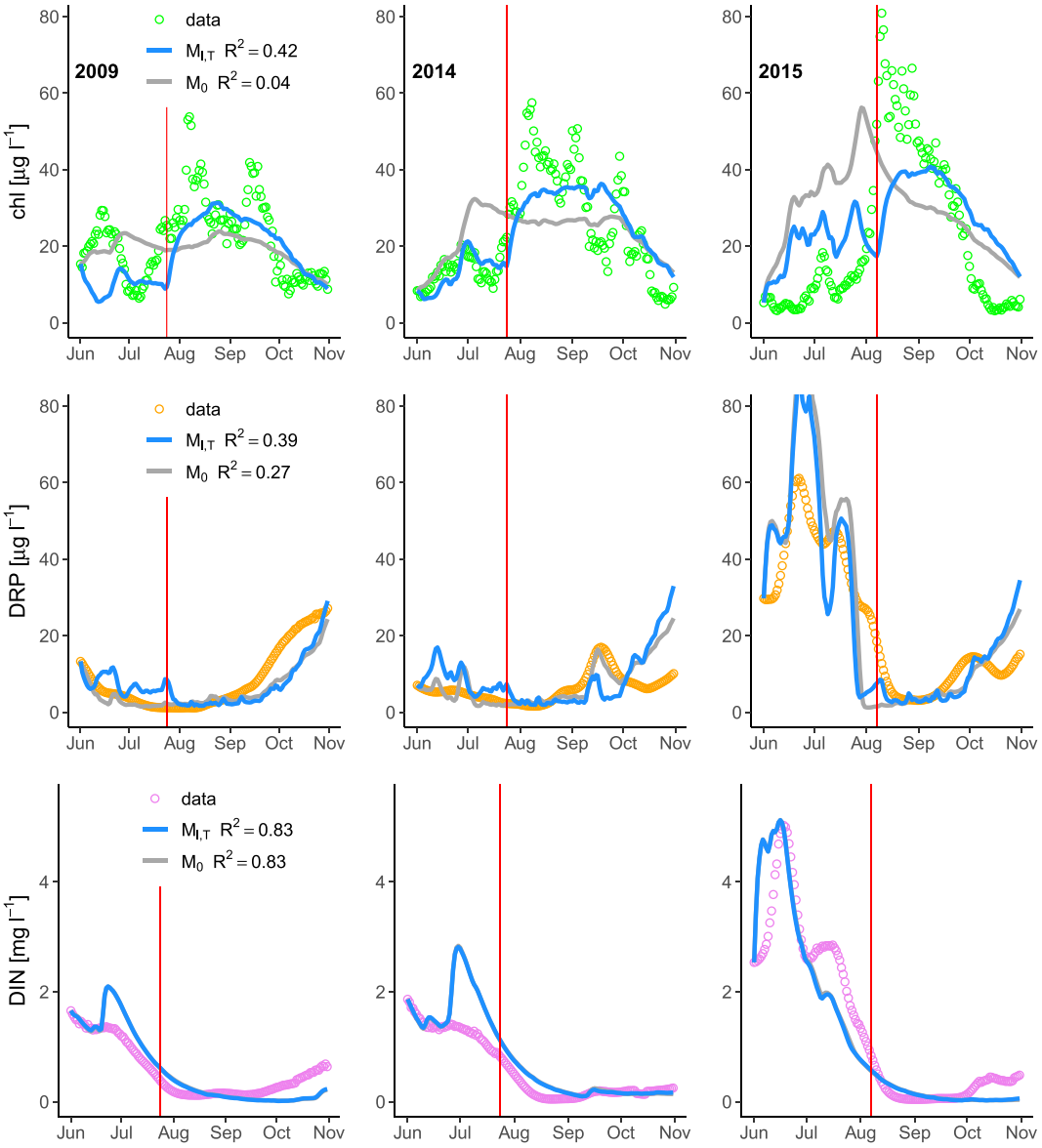

Fig. 5. Observed and modeled time series of lacustrine concentrations for same years as Fig. 3. The baseline model (M_0, gray) is compared to the final model ($M_{l,T}$, blue). This latter model has variable loss rates that are regulated by a temperature-dependent bloom initiation date (red vertical line represents the predicted initiation date, which is imperfect but represents a major improvement relative to M_0). Note that for DIN, the two models generate nearly identical outputs (such that the gray line is obscured). Also, R^2 values are for all years and 10-day data resolution, as used in the likelihood function. All studied years are presented in Figs. S3–S5 and cross-validation results with predictive uncertainty are displayed in Figs. S6–S8. (For interpretation of the references to colour in this figure legend, the reader is referred to the web version of this article.)

et al., 2012; Verhamme et al., 2016). Additionally, $M_{l,T}$ represents cyanobacterial dominance parsimoniously without explicitly parameterizing several phytoplankton groups. While ecologically complex models can be used to explore mechanisms in more detail, they can be challenging to parameterize and often have limited predictive capabilities (Nelson et al., 2020; Shimoda and Arhonditsis, 2016).

3.4. Model fit and predictive performance

Our final model ($M_{l,T}$) explains about 40% of the chl and DRP variability and over 80% of DIN variability (Table 2), on par with the performance of other mechanistic eutrophication models (Arhonditsis and Brett, 2004). Also, performance in terms of relative error (for chl = 0.5) is comparable or better than higher-resolution and mechanistically-complex phytoplankton models (e.g., relative error of 1.2–2.3, Sadeghian et al., 2018). Model predictive performance is further corroborated via out-of-sample validation. Specifically, we perform a leave-one-year-out cross-validation to test how well the median and 90% prediction intervals represent bloom characteristics (i.e. concentrations) in each year, while excluding that year from calibration. Validation results (Figs. S6–S8) show that out-of-sample performance is satisfactory (R^2 of about 0.30 for chl and DRP and 0.82 for N) and the coverage of the 90% bounds is close to optimal (89%, 85%, and 83%, for chl, DRP, and N, respectively).

The model also predicts the timing of bloom initiation consistent with our geostatistical estimates (Fig. 5) and other observational studies (Bridgeman et al., 2012; Stumpf et al., 2012). For example, we predict the 2013 bloom initiation on 25 July, consistent with remote sensing observations indicating the cyanobacteria bloom started between 21 and 30 July (Stumpf et al., 2016). In another example, Bosse et al. (2019) observed cyanobacterial dominance to start on roughly 4 August 2015 in the MPA, and NOAA reported a rapid increase in cyanobacteria during 3–6 August (https://www.glerl.noaa.gov/res/HABs_and_Hypoxia/lakeErieHABArchive/), consistent with our model-predicted bloom initiation date of 6 August 2015. Cross-validation also shows these bloom

initiation dates to be highly robust (e.g., 21 July and 6 August were determined for 2013 and 2015, respectively, when those years were omitted from the calibration).

However, aspects of specific blooms are not captured by our model. For example, blooms in 2012 and 2013 were more intense than simulated (Fig. S3). These years have also been identified as problematic when assessing relationships between nutrient loading and remotely sensed estimates of western basin bloom size (Stumpf et al., 2016). In our study, 2012 had the lowest spring (May–June) DRP and DIN loads, yet MPA chl concentrations were about average. On the other hand, 2013 had the highest peak MPA chl, yet spring loads were about average. The study of these anomalous years could be worth future research. At the same time, we note that both remote sensing and extracted chlorophyll provide indirect and imperfect estimates of HAB biomass with considerable uncertainty (e.g., Fang et al., 2019), such that exact matches to observed bloom measurements are not expected.

3.5. Inferred nutrient cycling and limitation rates

Because parsimonious mechanistic models can fit output variables well but with incorrect and compensating parameters (see e.g. discussion of model inadequacies in Reichert and Mieleitner (2009)), it is important to also explore inferred process rates of our final model. The estimated average sediment DRP flux is 0.21 ($\pm$0.04) μg l^{-1} d^{-1} or 0.63 mg m^{-2} d^{-1}, which is consistent with fluxes measured in the MPA (0.56–1.08 mg m^{-2} d^{-1}, Matisoff et al., 2016) and with phosphate fluxes used in previous algal models of LE (1 mg m^{-2} d^{-1}, Jiang et al., 2015). The estimated dissimilatory N reduction rate k_d (0.047 $\pm$ 0.002 d^{-1}), the major process for DIN removal in LE (Salk et al., 2018), is close to the 0.05 d^{-1} rate used by Sadeghian et al., (2018). The estimated remineralization rate ($k_m = 0.024 \pm 0.005$ d^{-1}) is between typical decay rates for labile and refractory particulate organic matter, which are 0.05 d^{-1} and 0.001 d^{-1}, respectively (Jiang et al., 2015; Sadeghian et al., 2018). The estimated effective settling rate of nonalgal biomass ($v_s = 0.015 \pm 0.005$ m d^{-1}) is lower than typical settling rates (0.25 m d^{-1}, Jiang et al., 2015). However, our value is logically slower because nonalgal biomass here includes zooplankton and thus implicitly takes into account the additional time needed for this living biomass to be processed before settling.

Nutrient limitation is influenced by the Monod half saturation parameters for P (S_p) and N (S_n) (Eq. (5)). In the final model, $M_{l,T}$, these concentrations are estimated to be 5.26 $\pm$ 0.7 and 13.7 $\pm$ 2.7 [μg l^{-1}], respectively (Fig. S2). Probabilistic predictions of nutrient limitation are obtained by propagating the posterior distribution of S_p and S_n through the model, thus considering their uncertainties. Our results show that in every summer, DRP is most commonly limiting algal production, with DIN often constraining algal growth toward the end of the season (on average, 26% of October days have probability of N limitation >50%, Fig. 6). This pattern reflects that autumn DRP concentrations typically increase faster than DIN (Fig. 5), consistent with bioassays showing P limitation followed by N limitation as summer proceeds (Chaffin et al., 2014). On average, 84% of the days between 1 June and 31 October show strong P limitation, 9% N limitation, and 7% little nutrient limitation (i.e., $\phi_N > 0.8$). We note that nutrient simulations are largely consistent across the different model versions (e.g., Fig. 5), suggesting that these nutrient limitation results are robust to variations in model form.

Nutrient limitation is most severe in early August (90% of the years due to P deficiency) when chl concentrations are particularly high. Interestingly, however, the most severe limitation appears to have occurred in early August 2012, when the algal growth rate was reduced by 86% due to scarcity of N (Fig. S9). That year also had the longest period of N limitation (30% of days), consistent with bioassays (Chaffin et al., 2014). Other years, such as 2008, show a high probability of continuous P limitation, consistent with cellular analyses (Chaffin et al., 2011).

In general, nutrient limitation patterns are consistent with our sensitivity analyses (conducted changing each riverine input individually by $\pm$20%, Fig. S10), showing that riverine P plays a key role in controlling LE algal concentration. Average lake chl is much less sensitive to changes in riverine DIN, including NH_3. Previous studies also corroborate the finding that algal biomass is principally influenced by P availability (Ho and Michalak, 2017; Obenour et al., 2014; Stumpf et al., 2016; Watson et al., 2016). At the same time, we note there is still debate on how nutrients regulate overall bloom size, with some studies emphasizing evidence in support of N limitation (Gobler et al., 2016; Newell et al., 2019) and others assigning preponderant importance to P (Scavia et al., 2016; Schindler et al., 2016). Additionally, beyond the question of phytoplankton growth limitation considered here,

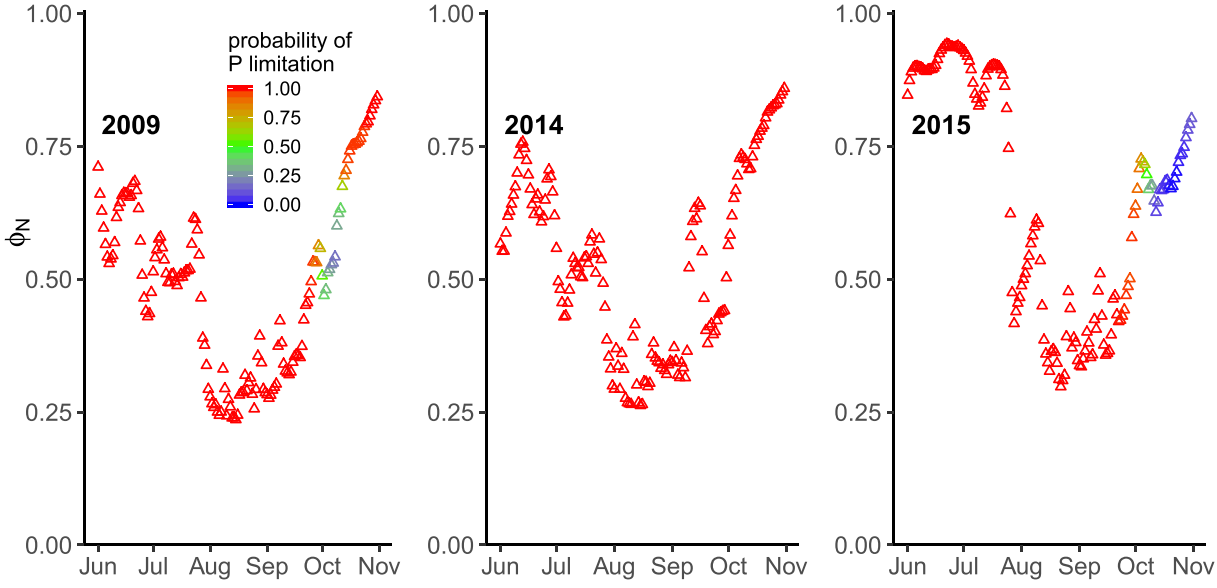

Fig. 6. Time series of overall nutrient limitation term ϕ_N, with colour providing a probabilistic assessment of the limiting nutrient. Results are based on the final model ($M_{l,T}$) using Eq. (5) and the posterior distributions in Fig. S2. Phosphorus has high probability of limiting overall algal growth most of the time, whereas nitrogen often becomes more limiting in early autumn. All studied years are shown in Fig. S9.

variations in the form (N vs. P) and intensity of nutrient limitation can regulate the dominance of different phytoplankton taxa (Reynolds, 2006). For example, N appears important for controlling cyanobacterial species composition and bloom toxicity (Gobler et al., 2016).

3.6. Temperature as a key driver of bloom initiation

Our analysis of environmental bloom triggers (Section 3.3) is consistent with other work that suggests temperature plays a key role in HAB regulation (Paerl and Otten, 2013), especially the timing of bloom initiation, which in LE is associated with a shift toward cyanobacteria dominance (Stumpf et al., 2012; Watson et al., 2016). This temperature effect is also consistent with findings from other lakes of similar latitude, for which algal blooms appear to occur earlier as warming increases (Peeters et al., 2007). We find that other meteorological variables such as wind have a less clear connection with bloom initiation, consistent with previous studies showing less strong relationships between algal blooms and wind velocity (Bertani et al., 2017; Peeters et al., 2007). Additionally, the importance of exceeding 20 °C in the model is consistent with literature on cyanobacterial blooms in LE (Bertani et al., 2017; Stumpf et al., 2016) and elsewhere (O'Neil et al., 2012; Robarts and Zohary, 1987).

Given the apparent importance of water temperature, we analyze the potential impact of a plausible climate-driven temperature increase on bloom initiation and biomass accumulation. We choose a + 2 °C temperature change that was used in previous eutrophication scenario analyses (e.g., Del Giudice et al., 2019), which is also consistent with the temperature increase to be expected around 2050 for LE in a 'business-as-usual' scenario (Del Giudice et al., 2018b). This ceteris paribus analysis shows that uniformly increasing historical water temperatures by 2 °C would lead to bloom initiation 10 ± 7 days earlier and would cause a 23 ± 9% increase in average summertime chl due to higher growth and mineralization rates, internal DRP flux, and longer periods of cyanobacteria dominance with reduced mortality.

The link between warm temperatures and early bloom initiation might be due to several mechanisms. First, higher temperatures may lead to cyanobacteria growth rates higher than those of competing phytoplankton groups (Huisman et al., 2018; Paerl and Otten, 2013). These differential temperature effects are commonly incorporated into models with multiple phytoplankton groups (e.g., Verhamme et al., 2016). However, the empirical foundation of this mechanism has been debated (Carey et al., 2012; Wagner and Adrian, 2009) and challenged by a meta-analysis indicating that cyanobacteria growth rates are not higher than those of other common algal groups, even at temperatures above 20 °C (Lürling et al., 2013).

Another mechanism for temperature-regulated bloom initiation is based on reduced zooplankton grazing at warmer temperatures (Kosten et al., 2012; Lürling et al., 2013). There is evidence that warming can lead to a reduction in zooplankton body size and grazing, including a decline in large cladocerans (Moore and Folt, 1993; Strecker et al., 2004), which are the main grazers of cyanobacteria (Lürling et al., 2013). This mechanism appears consistent with Twiss et al. (2014), who discussed that during non-summer months, grazing keeps the LE phytoplankton population at equilibrium, and that algal blooms could be initiated by a reduction of grazing pressure by large zooplankton.

A third mechanism by which temperature may regulate bloom initiation is through strengthening water column stability and stratification (Robarts and Zohary, 1987; Wagner and Adrian, 2009). On the one hand, the impact of stratification on MPA cyanobacteria is expected to be small because the MPA is shallow and frequently mixed (Bosse et al., 2019) with no clear effects of wind on bloom initiation (e.g., Fig. 4 and Bertani et al., 2017). However, Fang et al. (2019) showed that even for relatively shallow (3 m) areas of western LE, summertime algal concentrations can be elevated near the surface, likely due to temperature-induced water stability and cyanobacterial buoyancy. Indeed, Han et al. (2019) showed that warm quiescent summer conditions can be advantageous to cyanobacteria even in a shallow polymictic waterbody. Overall, there are multiple mechanisms by which increased temperature can promote cyanobacteria dominance, and it is likely that a combination of these factors lead to bloom initiation in western LE.

3.7. Reduced grazing as a mechanism for bloom accumulation following initiation

Results of our model experiments (Table 2) show that following bloom initiation, biomass accumulation is driven primarily by a downward shift in the loss rate rather than an upward shift in growth rate. Furthermore, time series of simulated growth rate adjustments (Fig. 7) show that, after mid-July, growth rates decrease dramatically

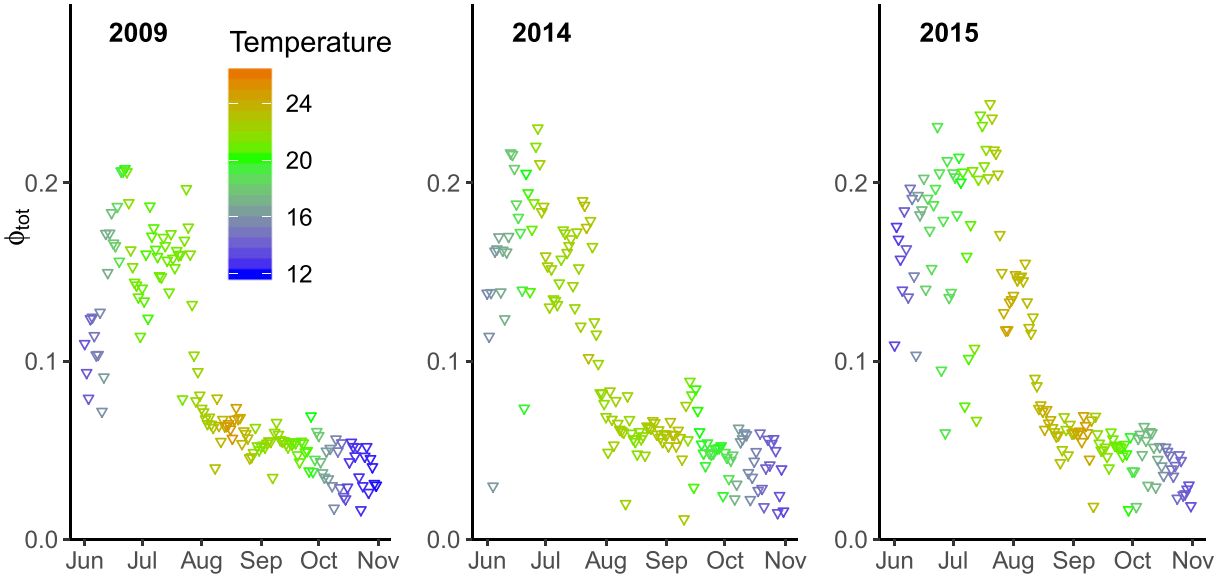

Fig. 7. Time series of total growth rate adjustment ($\phi_L\phi_N 1.066^{T-20}$ term in Eq. (1)) according to the final model ($M_{l,T}$). The highest growth rates generally occur in June and July, when nutrient concentrations are elevated (Fig. 6), irradiation is peaking, and water temperature is increasing (see Fig. S11 for all years).

even as temperature continues to increase, mostly because of severe nutrient shortages (Fig. 6) and self-shading of concentrated algal biomass (Eq. S1).

The importance of changes in loss rate due to reduced cyanobacteria grazing has been recognized in LE and other freshwater systems. During periods not dominated by cyanobacteria, Gobler et al. (2008) showed that the primary source of LE phytoplankton mortality is zooplankton grazing, and Lavrentyev et al. (2004) showed herbivory can exceed 90% of daily phytoplankton production in coastal areas of LE. The hypothesis of high herbivory keeping chl concentration low in early summer (despite high nutrient concentrations and growth rates) is also supported by observations (Conroy et al., 2017) and modeling results (Jiang et al., 2015) that show zooplankton biomass in LE coastal areas peaks around June.

In contrast, the low mortality rate we estimate under bloom conditions ($k_{l,b} \approx 0.1\ d^{-1}$, Fig. S2) is consistent with observations in western LE that show mesozooplankton grazing loss on cyanobacteria is about $0.06\ d^{-1}$ and with the tendency for grazing to decline as cyanobacterial density increases (Davis et al., 2012). This decline in zooplankton predation once cyanobacteria reach high density has been shown in other systems as well, and might be facilitated by algal toxicity and colonial structure (Paerl and Otten, 2013; Wagner and Adrian, 2009; De Stasio et al., 2018). Consistent with these observational studies, some mechanistic modeling studies deactivate the grazing loss for cyanobacteria (Chapra et al., 2017; Zhang et al., 2008). Compared to these previous studies, however, our approach demonstrates how long-term datasets can be used to statistically infer the magnitude and timing of this shift in grazing, which is critical to understanding and predicting bloom formation.

4. Summary and implications

In this study, we combine a mechanistically parsimonious model of phytoplankton dynamics, Bayesian inference, and a high temporal-resolution dataset to provide new insights into HAB development and nutrient cycling. Our results help explain the observed time lag between high nutrient concentrations and bloom initiation in Lake Erie. We suggest that, during early summer, high nutrient concentrations and mild temperatures favor rapid algal growth rates, yet phytoplankton biomass does not dramatically increase because of zooplankton grazing pressure.

Bloom initiation, typically occurring in late July, is associated with warmer temperatures that favor cyanobacteria. Once cyanobacteria are established, substantial biomass accumulation is driven primarily by reduced grazing rates. We additionally find that about one month of water temperatures continuously exceeding 20 °C is an apparent trigger for the reduced grazing associated with cyanobacteria dominance, substantially improving our ability to predict temporal bloom dynamics. While leave-one-year-out cross validation indicates robust model performance, our parameterization of bloom timing is based on just 10 years of data, such that future testing and refinement could be beneficial as more data become available. In general, modeling results indicate that warmer temperatures due to climate change will lead to earlier initiation of the HAB season and thus potentially extended disturbances to the health and economics of communities surrounding this and similar lakes. In this context, a reduction of nutrient loadings appears to be even more crucial to curb eutrophication and its undesirable consequences.

CRediT authorship contribution statement

Dario Del Giudice: Conceptualization, Methodology, Software, Formal analysis, Visualization, Writing - original draft. **Shiqi Fang:** Methodology, Software, Formal analysis. **Donald Scavia:** Conceptualization, Funding acquisition, Writing - review & editing. **Timothy W. Davis:** Writing - review & editing. **Mary Anne Evans:** Conceptualization, Writing - review & editing. **Daniel R. Obenour:** Conceptualization, Methodology, Supervision, Funding acquisition, Writing - review & editing.

Declaration of competing interest

The authors declare that they have no known competing financial interests or personal relationships that could have appeared to influence the work reported in this paper.

Acknowledgments

This work was supported by the National Science Foundation Coastal SEES grant (#OCE-1600012). Model code is available from the corresponding author on request. We appreciate Nathan Manning's help in obtaining NH_3 data from Heidelberg NCWQR. We also thank Caren Binding, Justin Chaffin, Thomas Bridgeman, and Thomas Johengen for assistance with in-lake sampling data. Finally, we are grateful to the reviewers for their constructive comments. Any use of trade, product, or firm names is for descriptive purposes only and does not imply endorsement by the U.S. Government.

Appendix A. Supplementary data

Supplementary data to this article can be found online at https://doi.org/10.1016/j.scitotenv.2020.142487.

References

Anderson, D.M., Cembella, A.D., Hallegraeff, G.M., 2012. Progress in understanding harmful algal blooms (HABs): paradigm shifts and new technologies for research, monitoring and management. Annu. Rev. Mar. Sci. 4, 143–176. https://doi.org/10.1146/annurev-marine-120308-081121.

Arhonditsis, G.B., Brett, M.T., 2004. Evaluation of the current state of mechanistic aquatic biogeochemical modeling. Mar. Ecol. Prog. Ser. 271, 13–26. https://doi.org/10.3354/meps271013.

Arhonditsis, G.B., Neumann, A., Shimoda, Y., Kim, D.-K., Dong, F., Onandia, G., Yang, C., Javed, A., Brady, M., Visha, A., Ni, F., Cheng, V., 2019. Castles built on sand or predictive limnology in action? Part A: evaluation of an integrated modelling framework to guide adaptive management implementation in Lake Erie. Ecol. Inform. 53, 100968. https://doi.org/10.1016/j.ecoinf.2019.05.014.

Bertani, I., Steger, C.E., Obenour, D.R., Fahnenstiel, G.L., Bridgeman, T.B., Johengen, T.H., Sayers, M.J., Shuchman, R.A., Scavia, D., 2017. Tracking cyanobacteria blooms: do different monitoring approaches tell the same story? Sci. Total Environ. 575, 294–308. https://doi.org/10.1016/j.scitotenv.2016.10.023.

Bosse, K.R., Sayers, M.J., Shuchman, R.A., Fahnenstiel, G.L., Ruberg, S.A., Fanslow, D.L., Stuart, D.G., Johengen, T.H., Burtner, A.M., 2019. Spatial-temporal variability of in situ cyanobacteria vertical structure in Western Lake Erie: implications for remote sensing observations. J. Gt. Lakes Res. 45, 480–489. https://doi.org/10.1016/j.jglr.2019.02.003.

Bridgeman, T.B., Chaffin, J.D., Kane, D.D., Conroy, J.D., Panek, S.E., Armenio, P.M., 2012. From river to lake: phosphorus partitioning and algal community compositional changes in Western Lake Erie. J. Gt. Lakes Res. 38, 90–97. https://doi.org/10.1016/j.jglr.2011.09.010.

Bridgeman, T.B., Chaffin, J.D., Filbrun, J.E., 2013. A novel method for tracking western Lake Erie Microcystis blooms, 2002–2011. J. Gt. Lakes Res. 39, 83–89. https://doi.org/10.1016/j.jglr.2012.11.004.

Britton, C.M., Dodd, J.D., 1976. Relationships of photosynthetically active radiation and shortwave irradiance. Agric. Meteorol. 17, 1–7. https://doi.org/10.1016/0002-1571(76)90080-7.

Bullerjahn, G.S., McKay, R.M., Davis, T.W., Baker, D.B., Boyer, G.L., D'Anglada, L.V., Doucette, G.J., Ho, J.C., Irwin, E.G., Kling, C.L., Kudela, R.M., Kurmayer, R., Michalak, A.M., Ortiz, J.D., Otten, T.G., Paerl, H.W., Qin, B., Sohngen, B.L., Stumpf, R.P., Visser, P.M., Wilhelm, S.W., 2016. Global solutions to regional problems: collecting global expertise to address the problem of harmful cyanobacterial blooms. A Lake Erie case study. Harmful Algae, Global Expansion of Harmful Cyanobacterial Blooms: Diversity, ecology, causes, and controls 54, 223–238. https://doi.org/10.1016/j.hal.2016.01.003.

Carey, C.C., Ibelings, B.W., Hoffmann, E.P., Hamilton, D.P., Brookes, J.D., 2012. Eco-physiological adaptations that favour freshwater cyanobacteria in a changing climate. Water Res. 46, 1394–1407. https://doi.org/10.1016/j.watres.2011.12.016.

Carmichael, W.W., 2001. Health effects of toxin-producing cyanobacteria: "the CyanoHABs.". Hum. Ecol. Risk Assess. Int. J. 7, 1393–1407. https://doi.org/10.1080/20018091095087.

Carmichael, W.W., Boyer, G.L., 2016. Health impacts from cyanobacteria harmful algae blooms: implications for the North American Great Lakes. Harmful Algae, Global

Expansion of Harmful Cyanobacterial Blooms: Diversity, ecology, causes, and controls 54, 194–212. https://doi.org/10.1016/j.hal.2016.02.002.
Carpenter, S.R., 2008. Phosphorus control is critical to mitigating eutrophication. Proc. Natl. Acad. Sci. U. S. A. 105, 11039–11040. https://doi.org/10.1073/pnas.0806112105.
Chaffin, J.D., Bridgeman, T.B., Heckathorn, S.A., Mishra, S., 2011. Assessment of Microcystis growth rate potential and nutrient status across a trophic gradient in western Lake Erie. J. Gt. Lakes Res. 37, 92–100. https://doi.org/10.1016/j.jglr.2010.11.016.
Chaffin, J.D., Bridgeman, T.B., Bade, D.L., 2013. Nitrogen constrains the growth of late summer Cyanobacterial blooms in Lake Erie. Adv. Microbiol. 3, 16–26. https://doi.org/10.4236/aim.2013.36A003.
Chaffin, J.D., Bridgeman, T.B., Bade, D.L., Mobilian, C.N., 2014. Summer phytoplankton nutrient limitation in Maumee Bay of Lake Erie during high-flow and low-flow years. J. Gt. Lakes Res. 40, 524–531. https://doi.org/10.1016/j.jglr.2014.04.009.
Chapra, S.C., 2008. Surface Water-Quality Modeling. Waveland Press, Long Grove, USA.
Chapra, S.C., Boehlert, B., Fant, C., Bierman, V.J., Henderson, J., Mills, D., Mas, D.M.L., Rennels, L., Jantarasami, L., Martinich, J., Strzepek, K.M., Paerl, H.W., 2017. Climate change impacts on harmful algal blooms in U.S. freshwaters: a screening-level assessment. Environ. Sci. Technol. 51, 8933–8943. https://doi.org/10.1021/acs.est.7b01498.
Conroy, J.D., Kane, D.D., Briland, R.D., Culver, D.A., 2014. Systemic, early-season Microcystis blooms in western Lake Erie and two of its major agricultural tributaries (Maumee and Sandusky rivers). J. Gt. Lakes Res. 40, 518–523. https://doi.org/10.1016/j.jglr.2014.04.015.
Conroy, J.D., Kane, D.D., Quinlan, E.L., Edwards, W.J., Culver, D.A., 2017. Abiotic and biotic controls of phytoplankton biomass dynamics in a freshwater tributary, estuary, and large lake ecosystem: Sandusky Bay (Lake Erie) chemostat. Inland Waters 7, 473–492. https://doi.org/10.1080/20442041.2017.1395142.
Davis, T.W., Koch, F., Marcoval, M.A., Wilhelm, S.W., Gobler, C.J., 2012. Mesozooplankton and microzooplankton grazing during cyanobacterial blooms in the western basin of Lake Erie. Harmful Algae 15, 26–35. https://doi.org/10.1016/j.hal.2011.11.002.
Davis, T.W., Stumpf, R., Bullerjahn, G.S., McKay, R.M.L., Chaffin, J.D., Bridgeman, T.B., Winslow, C., 2019. Science meets policy: a framework for determining impairment designation criteria for large waterbodies affected by cyanobacterial harmful algal blooms. Harmful Algae 81, 59–64. https://doi.org/10.1016/j.hal.2018.11.016.
De Stasio, B.T., Beranek, A.E., Schrimpf, M.B., 2018. Zooplankton-phytoplankton interactions in Green Bay, Lake Michigan: lower food web responses to biological invasions. J. Gt. Lakes Res. 44, 910–923. https://doi.org/10.1016/j.jglr.2018.05.020.
Del Giudice, D., Honti, M., Scheidegger, A., Albert, C., Reichert, P., Rieckermann, J., 2013. Improving uncertainty estimation in urban hydrological modeling by statistically describing bias. Hydrol. Earth Syst. Sci. 17, 4209–4225. https://doi.org/10.5194/hess-17-4209-2013.
Del Giudice, D., Muenich, R.L., McCahon Kalcic, M., Bosch, N.S., Scavia, D., Michalak, A.M., 2018a. On the practical usefulness of least squares for assessing uncertainty in hydrologic and water quality predictions. Environ. Model. Softw. 105, 286–295. https://doi.org/10.1016/j.envsoft.2018.03.009.
Del Giudice, D., Zhou, Y., Sinha, E., Michalak, A.M., 2018b. Long-term phosphorus loading and springtime temperatures explain interannual variability of hypoxia in a large temperate Lake. Environ. Sci. Technol. 52, 2046–2054. https://doi.org/10.1021/acs.est.7b04730.
Del Giudice, D., Matli, V.R.R., Obenour, D., 2019. Bayesian mechanistic modeling characterizes Gulf of Mexico hypoxia: 1968–2016 and future scenarios. Ecol. Appl. 00, e02032. https://doi.org/10.1002/eap.2032.
Dietzel, A., Reichert, P., 2014. Bayesian inference of a lake water quality model by emulating its posterior density. Water Resour. Res. 50, 7626–7647. https://doi.org/10.1002/2012WR013086.
Fang, S., Del Giudice, D., Scavia, D., Binding, C.E., Bridgeman, T.B., Chaffin, J.D., Evans, M.A., Guinness, J., Johengen, T.H., Obenour, D.R., 2019. A space-time geostatistical model for probabilistic estimation of harmful algal bloom biomass and areal extent. Sci. Total Environ. 695, 133776. https://doi.org/10.1016/j.scitotenv.2019.133776.
Faraway, J.J., 2015. Linear Models with R. 2nd Ed. CRC press.
FitzJohn, R., 2019. Odin: ode generation and integration. R package version 0.2.4. https://github.com/mrc-ide/odin.
Gobler, C.J., Davis, T.W., Deonarine, S.N., Saxton, M.A., Lavrentyev, P.J., Jochem, F.J., Wilhelm, S.W., 2008. Grazing and virus-induced mortality of microbial populations before and during the onset of annual hypoxia in Lake Erie. Aquat. Microb. Ecol. 51, 117–128. https://doi.org/10.3354/ame01180.
Gobler, C.J., Burkholder, J.M., Davis, T.W., Harke, M.J., Johengen, T., Stow, C.A., Van de Waal, D.B., 2016. The dual role of nitrogen supply in controlling the growth and toxicity of cyanobacterial blooms. Harmful Algae, Global Expansion of Harmful Cyanobacterial Blooms: Diversity, ecology, causes, and controls 54, 87–97. https://doi.org/10.1016/j.hal.2016.01.010.
Golnick, P.C., Chaffin, J.D., Bridgeman, T.B., Zellner, B.C., Simons, V.E., 2016. A comparison of water sampling and analytical methods in western Lake Erie. J. Great Lakes Res. 42 (5), 965–971. https://doi.org/10.1016/j.jglr.2016.07.031.
Haario, H., Saksman, E., Tamminen, J., 2001. An adaptive Metropolis algorithm. Bernoulli 7, 223–242.
Han, Y., Smithheart, J.W., Smyth, R.L., Aziz, T.N., Obenour, D.R., 2019. Assessing vertical diffusion and cyanobacteria bloom potential in a shallow eutrophic reservoir. Lake Reserv. Manag. 0, 1–17. https://doi.org/10.1080/10402381.2019.1697402.
Ho, J.C., Michalak, A.M., 2017. Phytoplankton blooms in Lake Erie impacted by both long-term and springtime phosphorus loading. J. Gt. Lakes Res. 43, 221–228. https://doi.org/10.1016/j.jglr.2017.04.001.
Hoagland, P., Anderson, D.M., Kaoru, Y., White, A.W., 2002. The economic effects of harmful algal blooms in the United States: estimates, assessment issues, and information needs. Estuaries 25, 819–837. https://doi.org/10.1007/BF02804908.
Huisman, J., Codd, G.A., Paerl, H.W., Ibelings, B.W., Verspagen, J.M.H., Visser, P.M., 2018. Cyanobacterial blooms. Nat. Rev. Microbiol. 16, 471. https://doi.org/10.1038/s41579-018-0040-1.
Jankowiak, J., Hattenrath-Lehmann, T., Kramer, B.J., Ladds, M., Gobler, C.J., 2019. Deciphering the effects of nitrogen, phosphorus, and temperature on cyanobacterial bloom intensification, diversity, and toxicity in western Lake Erie. Limnol. Oceanogr. 64, 1347–1370. https://doi.org/10.1002/lno.11120.
Jiang, L., Xia, M., Ludsin, S.A., Rutherford, E.S., Mason, D.M., Marin Jarrin, J., Pangle, K.L., 2015. Biophysical modeling assessment of the drivers for plankton dynamics in dreissenid-colonized western Lake Erie. Ecol. Model. 308, 18–33. https://doi.org/10.1016/j.ecolmodel.2015.04.004.
Katin, A., Del Giudice, D., Obenour, D.R., 2019. Modeling biophysical controls on hypoxia in a shallow estuary using a Bayesian mechanistic approach. Environ. Model. Softw., 120104491 https://doi.org/10.1016/j.envsoft.2019.07.016.
Kosten, S., Huszar, V.L.M., Bécares, E., Costa, L.S., Donk, E. van, Hansson, L.-A., Jeppesen, E., Kruk, C., Lacerot, G., Mazzeo, N., Meester, L.D., Moss, B., Lürling, M., Nõges, T., Romo, S., Scheffer, M., 2012. Warmer climates boost cyanobacterial dominance in shallow lakes. Glob. Chang. Biol. 18, 118–126. https://doi.org/10.1111/j.1365-2486.2011.02488.x.
Lavrentyev, P.J., McCarthy, M.J., Klarer, D.M., Jochem, F., Gardner, W.S., 2004. Estuarine microbial food web patterns in a Lake Erie coastal wetland. Microb. Ecol. 48, 567–577. https://doi.org/10.1007/s00248-004-0250-0.
Leon, L.F., Smith, R.E.H., Hipsey, M.R., Bocaniov, S.A., Higgins, S.N., Hecky, R.E., Antenucci, J.P., Imberger, J.A., Guildford, S.J., 2011. Application of a 3D hydrodynamic–biological model for seasonal and spatial dynamics of water quality and phytoplankton in Lake Erie. J. Gt. Lakes Res. 37, 41–53. https://doi.org/10.1016/j.jglr.2010.12.007.
Lürling, M., Eshetu, F., Faassen, E.J., Kosten, S., Huszar, V.L.M., 2013. Comparison of cyanobacterial and green algal growth rates at different temperatures. Freshw. Biol. 58, 552–559. https://doi.org/10.1111/j.1365-2427.2012.02866.x.
Matisoff, G., Kaltenberg, E.M., Steely, R.L., Hummel, S.K., Seo, J., Gibbons, K.J., Bridgeman, T.B., Seo, Y., Behbahani, M., James, W.F., Johnson, L.T., Doan, P., Dittrich, M., Evans, M.A., Chaffin, J.D., 2016. Internal loading of phosphorus in western Lake Erie. J. Gt. Lakes Res. 42, 775–788. https://doi.org/10.1016/j.jglr.2016.04.004.
Michalak, A.M., Anderson, E.J., Beletsky, D., Boland, S., Bosch, N.S., Bridgeman, T.B., Chaffin, J.D., Cho, K., Confesor, R., Daloğlu, I., DePinto, J.V., Evans, M.A., Fahnenstiel, G.L., He, L., Ho, J.C., Jenkins, L., Johengen, T.H., Kuo, K.C., LaPorte, E., Liu, X., McWilliams, M.R., Moore, M.R., Posselt, D.J., Richards, R.P., Scavia, D., Steiner, A.L., Verhamme, E., Wright, D.M., Zagorski, M.A., 2013. Record-setting algal bloom in Lake Erie caused by agricultural and meteorological trends consistent with expected future conditions. Proc. Natl. Acad. Sci. 110, 6448–6452. https://doi.org/10.1073/pnas.1216006110.
Milutinović, A., Živin, M., Zorc-Pleskovič, R., Sedmak, B., Šuput, D., 2003. Nephrotoxic effects of chronic administration of microcystins -LR and -YR. Toxicon 42, 281–288. https://doi.org/10.1016/S0041-0101(03)00143-0.
Moore, M., Folt, C., 1993. Zooplankton body size and community structure: effects of thermal and toxicant stress. Trends Ecol. Evol. 8, 178–183. https://doi.org/10.1016/0169-5347(93)90144-E.
Nelson, N.G., Muñoz-Carpena, R., Phlips, E., 2020. Parameter uncertainty drives important incongruities between simulated chlorophyll-a and phytoplankton functional group dynamics in a mechanistic management model. Environ. Model. Softw., 104708 https://doi.org/10.1016/j.envsoft.2020.104708.
Newell, S.E., Davis, T.W., Johengen, T.H., Gossiaux, D., Burtner, A., Palladino, D., McCarthy, M.J., 2019. Reduced forms of nitrogen are a driver of non-nitrogen-fixing harmful cyanobacterial blooms and toxicity in Lake Erie. Harmful Algae 81, 86–93. https://doi.org/10.1016/j.hal.2018.11.003.
Obenour, D.R., Gronewold, A.D., Stow, C.A., Scavia, D., 2014. Using a Bayesian hierarchical model to improve Lake Erie cyanobacteria bloom forecasts. Water Resour. Res. 50, 7847–7860. https://doi.org/10.1002/2014WR015616.
O'Neil, J.M., Davis, T.W., Burford, M.A., Gobler, C.J., 2012. The rise of harmful cyanobacteria blooms: the potential roles of eutrophication and climate change. Harmful Algae, Harmful Algae–The requirement for species-specific information 14, 313–334. https://doi.org/10.1016/j.hal.2011.10.027.
Paerl, H.W., Otten, T.G., 2013. Harmful cyanobacterial blooms: causes, consequences, and controls. Microb. Ecol. 65, 995–1010. https://doi.org/10.1007/s00248-012-0159-y.
Peeters, F., Straile, D., Lorke, A., Livingstone, D.M., 2007. Earlier onset of the spring phytoplankton bloom in lakes of the temperate zone in a warmer climate. Glob. Chang. Biol. 13, 1898–1909. https://doi.org/10.1111/j.1365-2486.2007.01412.x.
Reichert, P., Mieleitner, J., 2009. Analyzing input and structural uncertainty of nonlinear dynamic models with stochastic, time-dependent parameters. Water Resour. Res. 45 (10). https://doi.org/10.1029/2009WR007814.
Reynolds, C.S., 2006. Ecology of Phytoplankton. Cambridge University Press, Cambridge.
Robarts, R.D., Zohary, T., 1987. Temperature effects on photosynthetic capacity, respiration, and growth rates of bloom-forming cyanobacteria. N. Z. J. Mar. Freshw. Res. 21, 391–399. https://doi.org/10.1080/00288330.1987.9516235.
Sadeghian, A., Chapra, S.C., Hudson, J., Wheater, H., Lindenschmidt, K.-E., 2018. Improving in-lake water quality modeling using variable chlorophyll a/algal biomass ratios. Environ. Model. Softw. 101, 73–85. https://doi.org/10.1016/j.envsoft.2017.12.009.
Salk, K.R., Bullerjahn, G.S., McKay, R.M.L., Chaffin, J.D., Ostrom, N.E., 2018. Nitrogen cycling in Sandusky Bay, Lake Erie: oscillations between strong and weak export and implications for harmful algal blooms. Biogeosciences 15, 2891–2907. https://doi.org/10.5194/bg-15-2891-2018.
Scavia, D., DePinto, J.V., Bertani, I., 2016. A multi-model approach to evaluating target phosphorus loads for Lake Erie. J. Gt. Lakes Res. 42, 1139–1150. https://doi.org/10.1016/j.jglr.2016.09.007.
Schindler, D.W., Carpenter, S.R., Chapra, S.C., Hecky, R.E., Orihel, D.M., 2016. Reducing phosphorus to curb lake eutrophication is a success. Environ. Sci. Technol. 50, 8923–8929. https://doi.org/10.1021/acs.est.6b02204.

Shimoda, Y., Arhonditsis, G.B., 2016. Phytoplankton functional type modelling: running before we can walk? A critical evaluation of the current state of knowledge. Ecol. Model. 320, 29–43. https://doi.org/10.1016/j.ecolmodel.2015.08.029.

Sikorska, A.E., Del Giudice, D., Banasik, K., Rieckermann, J., 2015. The value of streamflow data in improving TSS predictions – Bayesian multi-objective calibration. J. Hydrol. 530, 241–254. https://doi.org/10.1016/j.jhydrol.2015.09.051.

Steele, J.H., 1965. Notes on some theoretical problems in production ecology. In: Goldman, C.R. (Ed.), Prim. Product. Aquat. Environ. Mem Inst Ital Idrobiol 18 Suppl. Univ Calif. Press, Berkeley, pp. 383–393.

Steffen, M.M., Davis, T.W., McKay, R.M.L., Bullerjahn, G.S., Krausfeldt, L.E., Stough, J.M.A., Neitzey, M.L., Gilbert, N.E., Boyer, G.L., Johengen, T.H., Gossiaux, D.C., Burtner, A.M., Palladino, D., Rowe, M.D., Dick, G.J., Meyer, K.A., Levy, S., Boone, B.E., Stumpf, R.P., Wynne, T.T., Zimba, P.V., Gutierrez, D., Wilhelm, S.W., 2017. Ecophysiological examination of the Lake Erie microcystis bloom in 2014: linkages between biology and the water supply shutdown of Toledo, OH. Environ. Sci. Technol. 51, 6745–6755. https://doi.org/10.1021/acs.est.7b00856.

Steffensen, D.A., 2008. Economic cost of cyanobacterial blooms. In: Hudnell, H.K. (Ed.), Cyanobacterial Harmful Algal Blooms: State of the Science and Research Needs, Advances in Experimental Medicine and Biology. Springer New York, New York, NY, pp. 855–865 https://doi.org/10.1007/978-0-387-75865-7_37.

Strecker, A.L., Cobb, T.P., Vinebrooke, R.D., 2004. Effects of experimental greenhouse warming on phytoplankton and zooplankton communities in fishless alpine ponds. Limnol. Oceanogr. 49, 1182–1190. https://doi.org/10.4319/lo.2004.49.4.1182.

Stumpf, R.P., Wynne, T.T., Baker, D.B., Fahnenstiel, G.L., 2012. Interannual variability of cyanobacterial blooms in Lake Erie. PLoS One 7, e42444. https://doi.org/10.1371/journal.pone.0042444.

Stumpf, R.P., Johnson, L.T., Wynne, T.T., Baker, D.B., 2016. Forecasting annual cyanobacterial bloom biomass to inform management decisions in Lake Erie. J. Gt. Lakes Res. 42, 1174–1183. https://doi.org/10.1016/j.jglr.2016.08.006.

Thieurmel, B., Elmarhraoui, A., 2019. Suncalc: Compute Sun Position, Sunlight Phases, Moon Position and Lunar Phase. R Package Version 0.5.

Twiss, M.R., Smith, D.E., Cafferty, E.M., Carrick, H.J., 2014. Phytoplankton growth dynamics in offshore Lake Erie during mid-winter. J. Gt. Lakes Res. 40, 449–454. https://doi.org/10.1016/j.jglr.2014.03.010.

Verhamme, E.M., Redder, T.M., Schlea, D.A., Grush, J., Bratton, J.F., DePinto, J.V., 2016. Development of the Western Lake Erie ecosystem model (WLEEM): application to connect phosphorus loads to cyanobacteria biomass. J. Gt. Lakes Res. 42, 1193–1205. https://doi.org/10.1016/j.jglr.2016.09.006.

Villez, K., Del Giudice, D., Neumann, M.B., Rieckermann, J., 2020. Accounting for erroneous model structures in biokinetic process models. Reliab. Eng. Syst. Saf. 203, 107075 ISSN 0951-8320. https://doi.org/10.1016/j.ress.2020.107075.

Wagner, C., Adrian, R., 2009. Cyanobacteria dominance: quantifying the effects of climate change. Limnol. Oceanogr. 54, 2460–2468. https://doi.org/10.4319/lo.2009.54.6_part_2.2460.

Watson, S.B., Miller, C., Arhonditsis, G., Boyer, G.L., Carmichael, W., Charlton, M.N., Confesor, R., Depew, D.C., Höök, T.O., Ludsin, S.A., Matisoff, G., McElmurry, S.P., Murray, M.W., Peter Richards, R., Rao, Y.R., Steffen, M.M., Wilhelm, S.W., 2016. The re-eutrophication of Lake Erie: harmful algal blooms and hypoxia. Harmful Algae 56, 44–66. https://doi.org/10.1016/j.hal.2016.04.010.

Westra, S., Thyer, M., Leonard, M., Kavetski, D., Lambert, M., 2014. A strategy for diagnosing and interpreting hydrological model nonstationarity. Water Resour. Res. 50, 5090–5113. https://doi.org/10.1002/2013WR014719.

Zhang, H., Culver, D.A., Boegman, L., 2008. A two-dimensional ecological model of Lake Erie: application to estimate dreissenid impacts on large lake plankton populations. Ecol. Model. 214, 219–241. https://doi.org/10.1016/j.ecolmodel.2008.02.005.